NASA Technical Memorandum 87047

Filter Induced Errors in Laser Anemometer Measurements Using Counter Processors

Lawrence G. Oberle and Richard G. Seasholtz
Lewis Research Center
Cleveland, Ohio

Prepared for the
International Laser Anemometry Symposium
ASME Winter Annual Meeting
Miami, Florida, November 17-21, 1985

NASA

FILTER INDUCED ERRORS IN LASER ANEMOMETER MEASUREMENTS USING COUNTER PROCESSORS

Lawrence G. Oberle and Richard G. Seasholtz
National Aeronautics and Space Administration
Lewis Research Center
Cleveland, Ohio 44135

ABSTRACT

Previous simulations of laser Doppler anemometer (LDA) systems have focused primarily on noise studies or biasing errors. Another possible source of error is due to the choice of filter types and filter cutoff frequencies.

In general, before it is applied to the counter portion of the signal processor, a Doppler burst is filtered to remove the pedestal and to reduce noise in the frequency bands outside the region in which the signal occurs. Filtering, however, can introduce errors into the measurement of the frequency of the input signal which leads to inaccurate results.

With the results of this paper it is possible to evaluate errors caused by signal filtering in an LDA counter-processor data acquisition system and to choose filters for a specific application which will reduce these errors.

NOMENCLATURE

A_S	amplitude of Doppler burst peak, counts/sample period
A_{dc}	DC or background component of Doppler burst, counts/sample period
F_l	lower cutoff frequency of the filter, cycles/sample period
F_u	upper cutoff frequency of the filter, cycles/sample period
f_D	Doppler frequency of the burst, cycles/sample period
G	maximum value of $\|H(f)\|$
H(f)	frequency response function of a given filter
$\|H(f)\|$	magnitude of H(f)
K	comparison switch constant (generally set to 10)
K_A	arbitrary constant (usually 3 or 4) for setting counter thresholds
N	number of cycles used in comparison testing
N_c	number of cycles used in Doppler frequency measurement
N_f	number of fringes in the burst
N_{bw}	noise bandwidth, cycles/sample period
P_n	noise power
P_s	mean signal power
r	comparison ratio, 1/2 or 5/8
SNR	peak signal to noise ratio
T_N	time interval between zero-crossing time at the end of the first cycle to exceed TH2 and the zero-crossing time at the end of the last cycle in the comparison envelope
T_{Nc}	time interval between zero-crossing time at the end of the first cycle to exceed TH2 and the zero-crossing time at the end of the last cycle in the measurement envelope
TH1	low counter threshold (K_A x background noise level)
TH2	high counter threshold (5 x TH1)
t_0	time of peak of Doppler burst
V	visibility of the burst
x(t)	time domain output of the photomultiplier
$\langle x(t) \rangle$	expected value of x(t)

σ rms noise

ϕ phase angle of Doppler burst

INTRODUCTION

To date, most LDA data acquisition system analyses have focussed on the errors caused by noise or biasing. This paper evaluates the errors caused by signal filtering through a computer simulation of the signal processing sequence.

In general, a Doppler burst is filtered before being applied to the counter-processor to remove the DC component (pedestal) and to reduce noise from outside the frequency region containing the Doppler signal. The ideal filter for this application possesses three significant characteristics (1): linear phase (sometimes stated as constant time delay) in the passband, constant amplitude in the passband, and infinite attenuation outside the passband. While an ideal filter is theoretically impossible, approximations to this ideal can be made. These approximations to the ideal are the general filter types analyzed herein.

Filter-induced errors can be divided into three broad categories which correspond to the lack of perfection in the previously mentioned characteristics. These error categories are as follows: skewing of the zero-crossings used in determining the input frequency, caused by nonlinear phase delay in the filter; biasing or preferential selection of certain frequencies in the passband, caused by ripples in the filter amplitude within the passband; and errors caused by insufficiently attenuated noise from outside the passband.

Adrian and Earley (2) evaluated LDA counter-processor performance as a function of the noise attributes of the signal received by the photomultiplier. Dopheide and Taux (1) compared the counter-processor to a transient recorder but did note that "electronic filtering of the Doppler signal introduces the most important systematic error" to the data acquisition process. Hosel and Rodi (3) emphasized noise induced errors and determined that noise errors were a function of the signal to noise ratio (SNR), the noise spectrum bandwidth, and the counter control parameters. Except for Dopheide and Taux, when electronic filtering was mentioned at all, it was assumed that the filtering being done was appropriate for the signals being measured. The emphasis of the work by Dopheide and Taux, however, centered on the comparison of two data acquisition techniques, rather than filter type and use.

DIGITAL SIMULATION OF SIGNAL PROCESSING WITH THE COUNTER-PROCESSOR

Doppler Burst

The output of the photomultiplier tube is assumed to be a Gaussian modulated sinusoidal wave of frequency equal to the Doppler frequency. It is further assumed that the seed particle velocity vector which generates this signal is parallel to the fringe normals of the measurement volume. The parameters that describe the burst are the amplitude A_S, the number of fringes N_f (equal to the number of cycles between e^{-2} intensity points), the visibility V, the Doppler frequency f_D, the time at the peak of the burst t_0, and the phase ϕ. The constant background level is A_{dc}. The photoelectron rate is then

$$x(t) = A_{dc} + A_s \left\{1 + V \cos\left[2\pi f_D (t - t_\phi) + \phi\right]\right\} \times e^{-1/2\left[4f_D(t-t_0)/N_f\right]^2} \quad (1)$$

which is shown in Fig. 1(a) (in the time domain), and in Fig. 1(b) (in the frequency domain as represented by the magnitude along the positive frequency axis). Assuming a "short-term" counting condition (4), the number of counts (photon events) in a given interval $(t-(dt/2), t+(dt/2))$ is approximately $x(t)\,dt$. The actual number of counts in each time interval dt has a Poisson probability distribution. The probability of k counts in the interval dt is

$$P(k,m) = \frac{m^k}{k!} e^{-m} \quad (2)$$

where m is the expected count at time t

$$m = x(t)\,dt \quad (3)$$

The Doppler burst of Fig. 1(a) with shot effect induced white noise added is shown in Figs. 1(c) and (d). Figures 1(e) and (f) show the signal after filtering with a bandpass filter. Figure 1 illustrates the desired elimination of the pedestal and the reduction of the noise. The number of visible fringes has a direct affect on the apparent performance of the filters. Figure 2 shows an exaggerated view of this affect. The Doppler frequency of the bursts was shifted upwards to the upper cutoff frequency of the filter to highlight the pedestal leakage. Figure 2(a) depicts the spectrum of a Dopple burst with $N_f = 4$, while Fig. 2(b) shows the spectrum of a Doppler burst of identical frequency with $N_f = 12$. As can be seen in Figs. 2(c) and (d) (showing the signals of Figs. 2(a) and (b), after filtering), the pedestal in the 4 fringe case is much less attenuated than its 12 fringe counterpart. This pedestal leakage can result in frequency measurements which are much lower than the actual Doppler frequency.

Filters

The filters were simulated using classical analog filter designs, with the low pass prototypes being used to calculate the high pass filters using the usual transformation (5). The conversion to the digital domain is done by sampling the complex frequency response of the analog filter which is equivalent to impulse invariance (6, p. 198). For this to be a valid procedure the impulse response must decay to near zero in the time record. The bandpass filters were formed by cascading low and high pass filters of the required types. A hardware realization of these bandpass filters would require that an amplifier be inserted between the filters to maintain an acceptable signal level.

Four five-pole filters were examined in an attempt to determine which of the three criteria were the most significant in terms of filter-induced errors. The Butterworth filter (Fig. 3(a)) was chosen because the low pass prototype provides a transfer function which is "maximally flat" in the passband, although this characteristic is not maintained in the transformation to create the bandpass filter. The Bessel filter (Fig. 3(b)) low pass prototype exhibits a transfer function which is "maximally flat" in terms of the time delay in the passband, but again, this highly linear phase characteristic is not maintained when the low pass filter is transformed to generate the bandpass filter (5). Finally, the Chebyshev filters were chosen as

examples of filters with transfer functions of the lowest order which meet the specified attenuation criteria. The 1-dB filter (Fig. 3(c)) is an example of a filter with a fast falloff outside the passband, and the 0.1-dB filter (Fig. 3(d)) is an example of a filter with a low ripple. As a result of the low ripple, the Chebyshev 0.1-dB filter also has a flat passband magnitude.

Signal Filtering Using Discrete Fourier Transform (DFT)

For the digital simulation, the time record $x(t)$ of the burst was represented as 1024 uniformly space samples. The Fourier transform of this record reveals the Doppler frequency. In this paper, the simulated frequencies are expressed in units of cycles per sample period. Consider a Doppler burst of frequency f_D sampled 25 times per cycle with $N_f = 8$ visible fringes. The Doppler frequency of this signal is then 1/25 or 0.04 cycles/sample period, and the burst width is $N_f/f_D = 8/0.04 = 200$ sample periods.

A scaling factor is used to relate these numbers to actual signals obtainable from an LDA system. For example, with a scaling factor of 10^9 sample periods/second, the 0.04 cycles/sample period signal would correspond to a signal of frequency 40 MHz. The burst width would then be 200 sample periods/10^9 sample periods/second or 200 nsec in a time record of 1.024 μsec.

Because of the Nyquist criterion, the Doppler signal must be sampled at least twice per cycle to avoid aliasing in the reconstructed time record. This puts an upper limit on the simulated Doppler signal of 0.5 cycles/sample period. One would prefer to sample the signal on the order of 10 times/cycle, yielding an effective upper limit of 0.1 cycles/sample period. Furthermore, in order to use discrete Fourier transform to perform linear convolutions without aliasing, the sum of lengths of the nonzero portions of the Doppler burst and the nonzero portion of the impulse response of the filter must be less than the length of the time record (6, p. 111). This constraint places a lower limit on the frequencies to be studied using this simulation.

A ratio of upper to lower cutoff frequencies of 2 to 1 was considered general enough to serve the purposes of this paper. The upper cutoff frequency of the filters was chosen as 0.08 cycles/sample period to fall well within the upper frequency limit. The lower cutoff frequency was therefore 0.04 cycles/sample period. With the two cutoff frequencies specified, the impulse response of the filter (equal to the inverse discrete Fourier transform of the frequency responses of the filters) could be calculated. It was found that for the four filters, these functions approach zero at or about 256 sample periods. The nonzero portion of the Doppler burst could then extend to 750 sample periods and still meet the convolution constraint. This leads to a lower frequency limit on the Doppler burst (for $N_f = 8$) of $f_D = N_f/\text{length} = 8/750 = 0.011$ cycles/sample period. Since the frequencies of interest fall well within the range of 0.011 to 0.1 cycles/sample period, the frequency limits imposed by the Nyquist criterion and the discrete Fourier transform are satisfied.

Counter-Processor Simulation

The filtered signal, either noise-free or noise-added, is then applied to the counter simulation program. The algorithm for the processor is based on a commercially available signal processor used at NASA Lewis for laser Doppler Anemometry (LDA) measurements (7). The processor model performs two primary functions - input conditioning and timing.

Input conditioning can be viewed as defining the envelopes used in making the measurement. These envelopes are the burst envelope, the envelope of the number of cycles used in calculating the average (the N_C envelope), and the comparison envelope. The burst envelope detector determines the beginning and end of a Doppler burst using the thresholds TH1 and TH2 as shown in Fig. 4. The lower counter threshold TH1 is set to K_A times the background noise level, where K_A is an arbitrary constant. The high threshold TH2 is usually set to five times TH1. The beginning of the burst is defined as the first Doppler cycle which crosses TH2. The burst continues until a cycle crosses TH1 but not TH2. In Fig. 4, the burst envelope encompasses six valid cycles. The N_C envelope starts at the first valid cycle and continues until N_C cycles are found. This is shown in Fig. 4 for $N_C = 4$. If the burst ends before N_C cycles are found, the burst is ignored by the processor. The comparison envelope is defined in the same way as the N_C envelope but with fewer cycles. The ratio of the number of cycles in the comparison envelope to the number of cycles in the N_C envelope (called the comparison ratio r) is generally set to 1/2 for $N_C = 2$ and $N_C = 4$ and to 5/8 for $N_C = 3$. Figure 4 shows the comparison envelope applicable for $N_C = 4$.

The timing portion of the model uses the negative-going zero-crossings of the valid cycles (circled locations in Fig. 4) to determine the Doppler frequency. These zero-crossings are found using linear interpolation between the time domain samples that bracket the zero-crossing. In the actual processor, Schmitt triggers are used to find the zero-crossings. The Doppler frequency is then calculated as

$$f_D = \frac{N_C}{T_{Nc}} \tag{4}$$

where T_{NC} is the time interval between the first and last zero-crossings within the N_C envelope.

To determine if the Doppler frequency is changing drastically from cycle to cycle within the burst, a comparison test is made. T_N is defined as the time interval between the first and last zero-crossing in the comparison envelope. In the actual processor, the measurement passes the comparison test if

$$rT_{Nc} - K < T_N < rT_{Nc} + K \tag{5}$$

where K is a constant number of clock counts set from the front panel. For the simulation program, the comparison test uses the relationship

$$\left|rT_{Nc} - T_N\right| < \text{comparison accuracy} \tag{6}$$

where the comparison accuracy used is generally set to 5 percent. The simulation comparison test is percentage based, while the actual processor measures the difference in counts. What this implies is that in the real processor, as the Doppler frequency increases, the tolerance on the comparison validation increases because the limits are a fixed number of clock counts. In the digital simulation, the comparison validation is given as a percentage of T_{Nc}. The comparison was performed in this manner so as to generalize the results of this paper. To relate the percentage to the actual processor switch setting, the Doppler frequency must be specified.

Signal to Noise Ratio (SNR)

Since the noise output of the photomultiplier is assumed to be white, one cannot speak of SNR until the signal has been filtered. Herein, we define the peak SNR as the ratio of the mean signal power at the filter output to the filtered mean noise power where both are

averaged over one cycle, with the exponential term appearing in Eq. (1) set to its peak value, unity. Therefore, the mean signal power can be written as

$$P_s = 0.5(A_s V)^2 |H(f)|^2 \tag{7}$$

With the assumption of shot effect induced white noise, the power spectral density (at a given time) is equal to the expected photoelectron rate. The noise power is

$$P_n = 2 \langle x(t) \rangle N_{bw} \tag{8}$$

where the noise bandwidth N_{bw} is

$$N_{bw} = \frac{1}{G^2} \int_0^\infty |H(f)|^2 \, df \tag{9}$$

and G is defined as the maximum value of $|H(f)|$. Note that the rms noise (ensemble average at a given time) is

$$\sigma = \sqrt{P_n} \tag{10}$$

The noise power averaged over one cycle is thus

$$P_n = 2N_{bw}\left(A_{dc} + A_s\right) \tag{11}$$

and the peak SNR is

$$SNR = \frac{(A_s V)^2 |H(f)|^2}{4N_{bw}\left(A_{dc} + A_s\right)} \tag{12}$$

RESULTS

The output of the filter was determined by finding the inverse Fourier transform of the product of the Fourier transform of the input signal and the Fourier transform of the filter. The noise-free signals were evaluated primarily to determine the ability of the filters to attenuate the pedestal without affecting the Doppler frequency. As shown in Fig. 2, pedestal leakage is a strong function of N_f. However, it is not clear whether the pedestal leakage is a problem in determining the Doppler frequency.

A more obvious source of error in measurements is the number of cycles used in calculating the Doppler frequency. Figure 5 depicts the percent error as a function of frequency of the average of four fringes (i.e., $N_c = 4$) for $N_f = 4$, 8, and 12. It is apparent that one should not choose N_f to be equal to N_c, even if the flow is parallel to the fringe normals. Either the amplitude is not large enough to allow the four cycles to be counted (as is the case with the Bessel filter, Fig. 5(b)), or the error in the later cycles is large enough to induce relatively large errors in the average (as happens with the other filters). Otherwise, the general trend is that the larger the number of fringes, the more accurate the measurement will be. Other considerations, such as the size of the measurement volume, force the number of fringes to be as small as possible. It was our experience that if N_f is chosen to be roughly twice N_c, the measurement accuracy is sufficient. For purposes of this report, it was determined that the combination of $N_f = 8$ and $N_c = 4$ was adequate. These values will be used throughout the remainder of the report.

Another observation can be made from Fig. 5. The Butterworth filter frequency response exhibits a marked slope as a function of frequency. This implies that the measured frequency will tend to be biased toward the center of the filter passband. It is desirable that the slope of the error curve be very nearly flat over a wide range in the passband. The Bessel and both Chebyshev filters more nearly approach this condition. However, the slopes of the error curves in the Chebyshev filters become pronounced at the passband edges.

Table I shows the normalized frequency for individual cycles of the filtered bursts as a function of both frequency and filter. The amplitude was increased in each case until 10 cycles were accepted by the counter processor. In general, the later cycles result in a lower frequency than the earlier cycles, and the bursts of higher input frequency are biased toward the lower frequencies. The exceptions to these general trends are the two Chebyshev filters. At the higher frequencies, the later cycles are of higher frequency than the earlier cycles. This does not appear in the averages because bursts of high enough amplitude to be processed first cross TH2 (see Fig. 4) at cycle 4 or earlier. Those bursts which cross the upper threshold at cycle 5 or higher will not have 4 consecutive cycles at greater amplitude than TH2.

As noise is added to the Doppler signal, a number of observations can be made. Figure 6 is the comparison of normally distributed random amplitude signals (mean value equals 10 counts/sample period, standard deviation equals 10 counts/sample period), both noise-free and noise-added, as a function of frequency. For the noise-free case, the Bessel filter and the 0.1-dB Chebyshev filter appear less sensitive to amplitude fluctuations than the other two. But, again, for the four filters, the general trend is downward as the frequency increases. With Poisson-noise added, the signal accuracy deteriorates, as expected. The "bumps" in the Bessel filter frequency response occur because fewer bursts are accepted by the processor for this filter than for the other three. Since the Bessel filter attenuates the input signal, signals of higher input amplitude are necessary to cross the upper threshold. The data rate using the Bessel filter will be necessarily lower than for the other filters. The 0.1-dB Chebyshev filter exhibits the flattest profile throughout the frequency range.

Another consideration in the use of laser anemometers is the measurement of turbulence intensity. Figure 7 shows the standard deviation of the measurements as a function of frequency for the four filters for random amplitude signal with noise added. The four filters are clustered around the 1- to 1.5-percent range. This implies that turbulence intensities of this magnitude cannot be measured accurately using the standard techniques. Also, measurements of mean velocity will be biased near the band edges because of the variation of the measurement rate with frequency caused by filter attenuation. For these measurements, the Bessel filter exhibits the highest standard deviation at the higher frequencies. It is desirable that this curve be nearly flat to avoid errors in turbulence intensity as a function of frequency. The flattest profile can be seen to be the Butterworth filter, especially in the center of the passband, although the differences between these filters in this respect are not especially significant.

Figure 8 shows the SNR of the four filters as a function of frequency for fixed-amplitude, noise added input signals. The Bessel filter exhibits the least variation in SNR across the passband, but the SNR is significantly lower than for the other filters. The 0.1-dB Chebyshev filter also has a fairly flat profile,

but at higher magnitude than the Bessel. Both the Butterworth and the 1-dB Chebyshev filters exhibit a large variation of SNR as a function of frequency. This implies that the input signals will be biased more strongly by these filters than by the Bessel and the 0.1-dB Chebyshev filters. This observation is borne out by the graphs of Fig. 6.

CONCLUSIONS

From this admittedly limited study, several important conclusions can be reached. First, the error in the signal can be viewed to be partially a function of the ratio between N_f and N_c. As a rule of thumb, if $N_f/N_c \approx$ _, the errors caused by the large variation in cycle frequencies at the end of the burst will be minimized. Second, for the four filters studied, there is generally strong signal biasing near the band edges. This can be avoided by defining "effective" cutoff frequencies inside the actual cutoff frequencies of the filters. A 10-percent shift upwards for the low edge, and downwards for the high edge, should be sufficient to limit these errors. Third, biasing errors caused by the filters can be linked to the variations in SNR across the passband. A filter with a flat SNR profile is then more desirable than a filter with a large variation in SNR as a function of frequency. Fourth, variations in standard deviations, which can cause errors in turbulence intensity measurements, can be interpreted as a function of the magnitude of the SNR of the filtered signal. For this reason, and for the obvious reason that a higher SNR yields a higher data rate, a filter should be chosen which allows as high an SNR as possible. With these four points in mind, the Chebyshev filter with the 0.1-dB ripple is the best filter of the four studied.

It should be noted that this study is by no means exhaustive. No effort was made to determine the errors induced by these filters on the measurement of turbulent flow or of flows for which the mean velocity vector crosses the measurement volume at an angle to the fringe normals. Furthermore, there exist a large number of filters not evaluated here as well as higher order filters of the types examined. A more extensive study of these systematic errors is required to minimize the inaccuracies of the measurements made by fringe-type laser anemometry systems.

REFERENCES

1. Dopheide, D., and Taux, G. " Accurate Frequency Measurements of Noise-Added Doppler Signals by Means of Transient Recorders and LDA Counters Using a Laser Diode Simulator," Second International Symposium of Applications of Laser Anemometry to FTuid Mechanics, Lisbon, Portugal, 1984, pp. 4.3 to 4.3-7.
2. Adrian, R.J., and Early, W.L. "Evaluation of LDV Performance Using Mie Scattering Theory," Minnesota Symposium of Laser Anemometry, Univ. of Minnesota, Bloomington, MN, 1975, pp. 426-454.
3. Hosel, W., and Rodi, W. "Errors Occurring in LDA-Measurements with Counter Signal Processing," The Accuracy of Flow Measurements by Laser Doppler Methods, Skovlunde, Copenhagen, Denmark, 1975, pp. 251-257.
4. Gagliardi, R.M., and Karp, S., Optical Communications, Wiley, New York, 1976, p. 63.
5. Weinburg, L., Network Analysis and Synthesis, McGraw-Hill, New York, 1962, p. 535.
6. Oppenheim, A.V., and Schafer, R.W., Digital Signal Processing, Prentice-Hall, Englewood Cliffs, NJ, 1975.
7. "Instruction Manual, Model 1990 Counter Type Signal Processor for Laser Velocimeter," TSI P/N 1990147, TSI Inc., St. Paul, MN.

TABLE 1. - NORMALIZED FREQUENCY FOR INDIVIDUAL CYCLES OF FILTERED SIGNAL

BE = Bessel
BW = Butterworth
CH = Chebyshev

BANDPASS FILTER CUTOFF FREQUENCIES
Fl = .040 cycles/sample period
Fu = .080 cycles/sample period

Number fringes (Nf) = 8

Fd cycles/ sample period	filter	CYCLE 1	2	3	4	5	6	7	8	9	10
.040	BE	1.008	1.007	1.006	1.005	1.004	1.003	1.001	1.000	0.998	0.997
	BW	1.017	1.017	1.016	1.016	1.015	1.014	1.012	1.010	1.008	1.004
	CH-1dB	1.026	1.026	1.026	1.025	1.024	1.021	1.018	1.014	1.009	1.006
	CH-.1dB	1.017	1.016	1.014	1.012	1.008	1.003	0.996	0.986	0.970	0.948
.045	BE	1.006	1.005	1.004	1.003	1.002	1.001	1.000	0.999	0.997	0.995
	BW	1.012	1.011	1.010	1.009	1.007	1.005	1.002	0.997	0.992	0.984
	CH-1dB	1.016	1.015	1.013	1.009	1.004	0.996	0.983	0.963	0.930	0.891
	CH-.1dB	1.011	1.009	1.007	1.004	0.999	0.994	0.987	0.977	0.963	0.941
.050	BE	1.004	1.004	1.003	1.002	1.001	1.000	0.999	0.998	0.996	0.995
	BW	1.008	1.007	1.006	1.004	1.002	1.000	0.996	0.993	0.987	0.981
	CH-1dB	1.011	1.009	1.006	1.003	0.998	0.992	0.985	0.978	0.985	1.184
	CH-.1dB	1.007	1.006	1.004	1.001	0.998	0.995	0.992	0.991	0.993	1.000
.055	BE	1.003	1.003	1.002	1.001	1.000	1.000	0.998	0.997	0.995	0.994
	BW	1.006	1.005	1.004	1.003	1.001	1.000	0.998	0.995	0.993	0.991
	CH-1dB	1.007	1.006	1.004	1.001	0.999	0.996	0.994	0.995	0.999	0.995
	CH-.1dB	1.006	1.005	1.004	1.002	1.000	0.999	0.997	0.995	0.994	0.994
.060	BE	1.002	1.002	1.000	1.000	0.999	0.999	0.998	0.996	0.993	0.990
	BW	1.004	1.002	1.002	1.000	0.999	0.998	0.996	0.995	0.995	0.994
	CH-1dB	1.004	1.003	1.003	1.001	1.000	0.998	0.995	0.991	0.986	0.978
	CH-.1dB	1.005	1.003	1.003	1.001	1.000	0.999	0.997	0.996	0.995	0.992
.065	BE	1.001	1.001	0.999	0.999	0.999	0.998	0.998	0.996	0.991	0.986
	BW	1.000	1.000	0.998	0.997	0.997	0.995	0.995	0.994	0.994	0.997
	CH-1dB	1.001	1.000	1.001	1.001	1.001	1.002	1.003	1.003	1.000	0.978
	CH-.1dB	1.002	1.002	1.001	1.001	1.000	0.999	0.999	0.999	0.996	0.995
.070	BE	1.000	0.999	0.999	0.998	0.997	0.997	0.998	0.996	0.988	0.981
	BW	0.996	0.997	0.996	0.994	0.993	0.993	0.991	0.991	0.993	0.992
	CH-1dB	0.997	0.997	0.997	0.999	1.002	1.008	1.019	1.040	1.085	1.157
	CH-.1dB	0.999	1.000	0.999	0.999	1.000	1.001	1.002	1.003	1.004	1.006
.075	BE	1.000	0.998	0.998	0.997	0.996	0.997	0.998	0.995	0.989	0.967
	BW	0.994	0.994	0.991	0.991	0.990	0.988	0.988	0.985	0.986	0.985
	CH-1dB	0.989	0.990	0.990	0.990	0.994	0.998	1.007	1.021	1.037	1.052
	CH-.1dB	0.998	0.996	0.996	0.997	0.997	0.999	1.003	1.008	1.016	1.031
.080	BE	1.000	0.997	0.997	0.995	0.996	0.996	0.998	0.996	0.987	0.954
	BW	0.990	0.991	0.988	0.987	0.986	0.983	0.982	0.979	0.976	0.974
	CH-1dB	0.981	0.980	0.978	0.977	0.977	0.979	0.981	0.985	0.989	0.989
	CH-.1dB	0.991	0.993	0.992	0.993	0.994	0.998	1.002	1.012	1.027	1.045

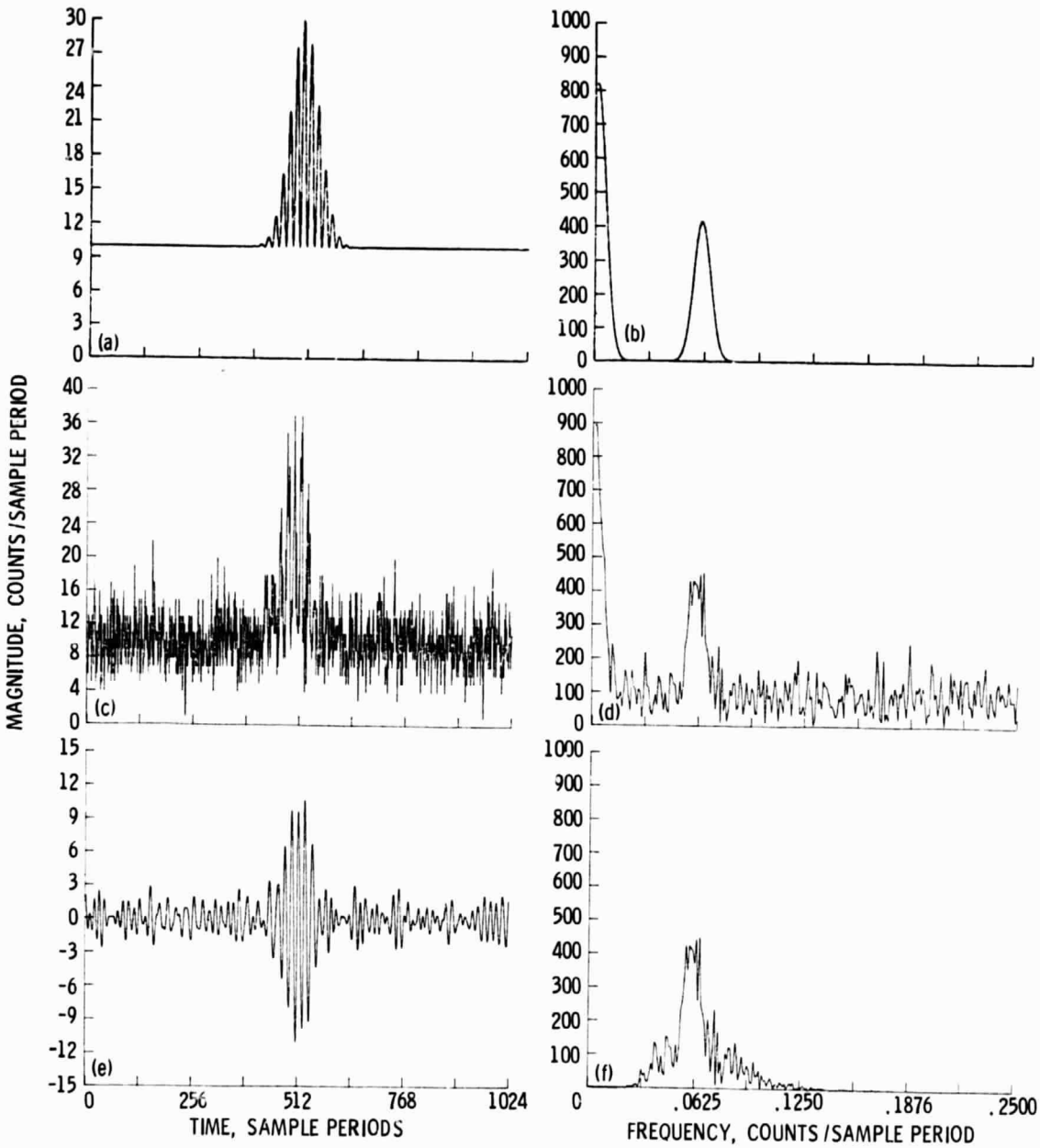

Fig. 1 Digital time records and frequency spectrum simulations of Doppler burst ($f_D = 0.060$; $A_{dc} = 10$ counts/sample period; $A_s = 10$ counts/sample period; $V = 1.0$; $N_f = 8$; $t_0 = 512$; $\varphi = 0.23475$ rad.)

(a) Noise-free time record
(b) Noise-free frequency spectrum
(c) Poisson noise-added time record
(d) Noise-added frequency spectrum
(e) Time record of noise-added signal filtered by Chebyshev filter (0.1 dB) ($F_l = 0.04$ cycles/sample period; $F_u = 0.08$ cycles/sample period)
(f) Frequency spectrum of noise-added filtered signal

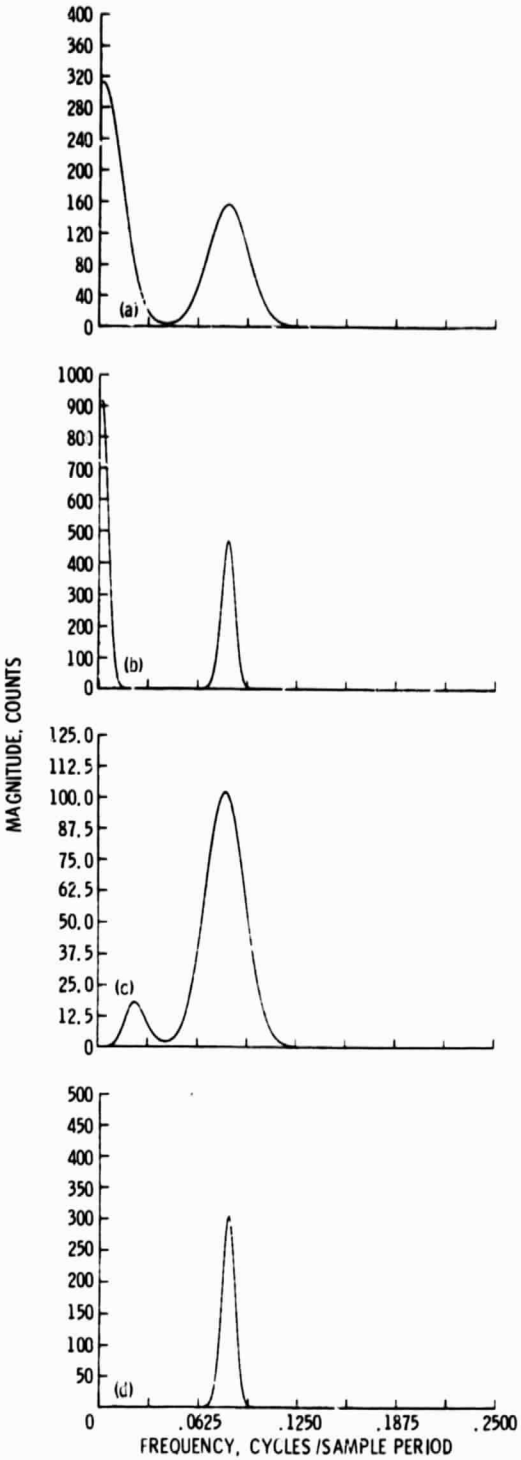

Fig. 2 Frequency spectrum of Doppler burst showing effect of N_f on pedestal leakage (f_D = 0.08 cycles/sample period)

(a) Unfiltered frequency spectrum with N_f = 4

(b) Unfiltered frequency spectrum with N_f = 12

(c) Signal from (a) filtered with Bessel filter (F_l = 0.04 cycles/sample period; F_u = 0.08 cycles/sample period)

(d) Signal from (b) filtered with Bessel filter (F_l = 0.04 cycles/sample period; F_u = 0.08 cycles/sample period)

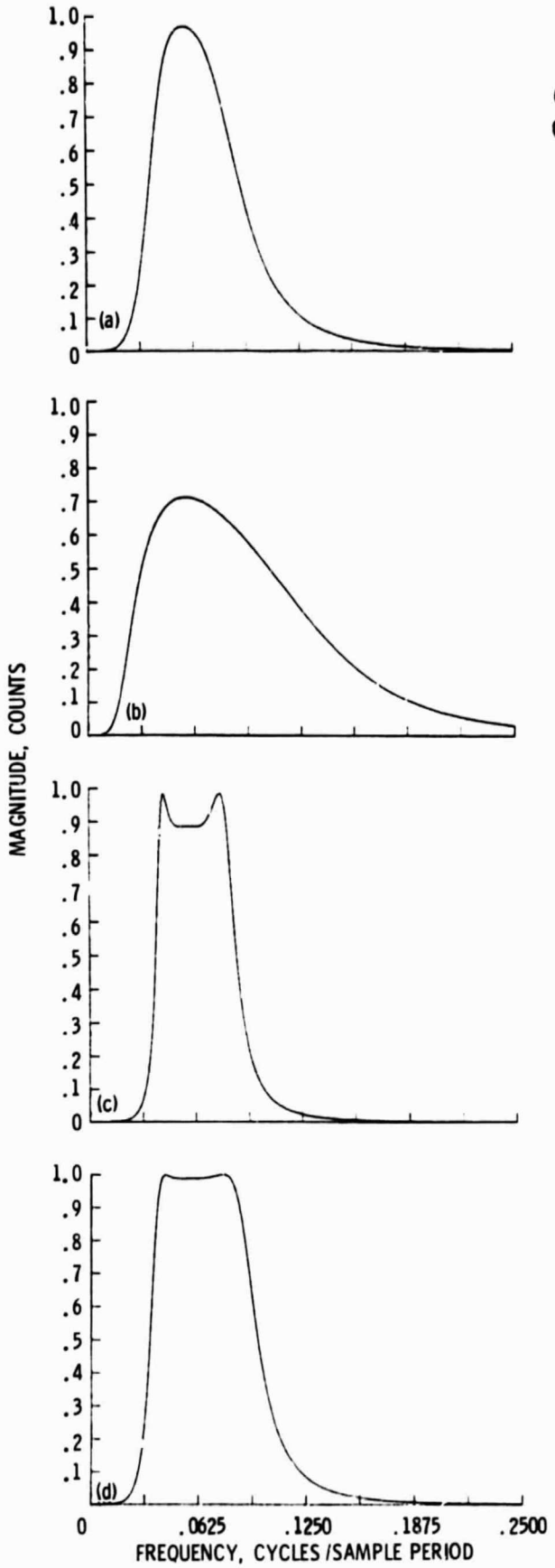

Fig. 3 Magnitude of frequency response of four filters (five pole; F_l = 0.04 cycles/sample period; F_u = 0.08 cycles/sample period)

(a) Butterworth filter
(b) Bessel filter
(c) Chebyshev filter (10-dB ripple)
(d) Chebyshev filter (0.1-dB ripple)

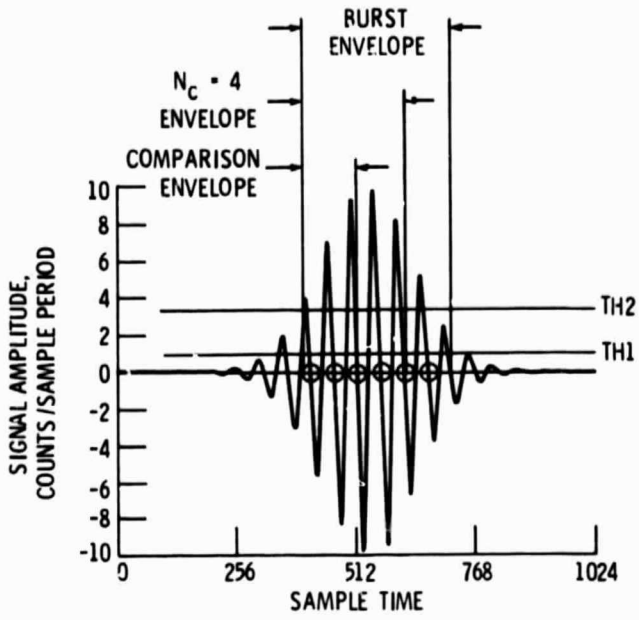

Fig. 4 Measurement of Doppler frequency by counter-processor (processor measures elapsed time for zero crossings of N_C cycles that cross upper threshold (TH2). Shown are burst envelope, N_C envelope, and comparison envelope.)

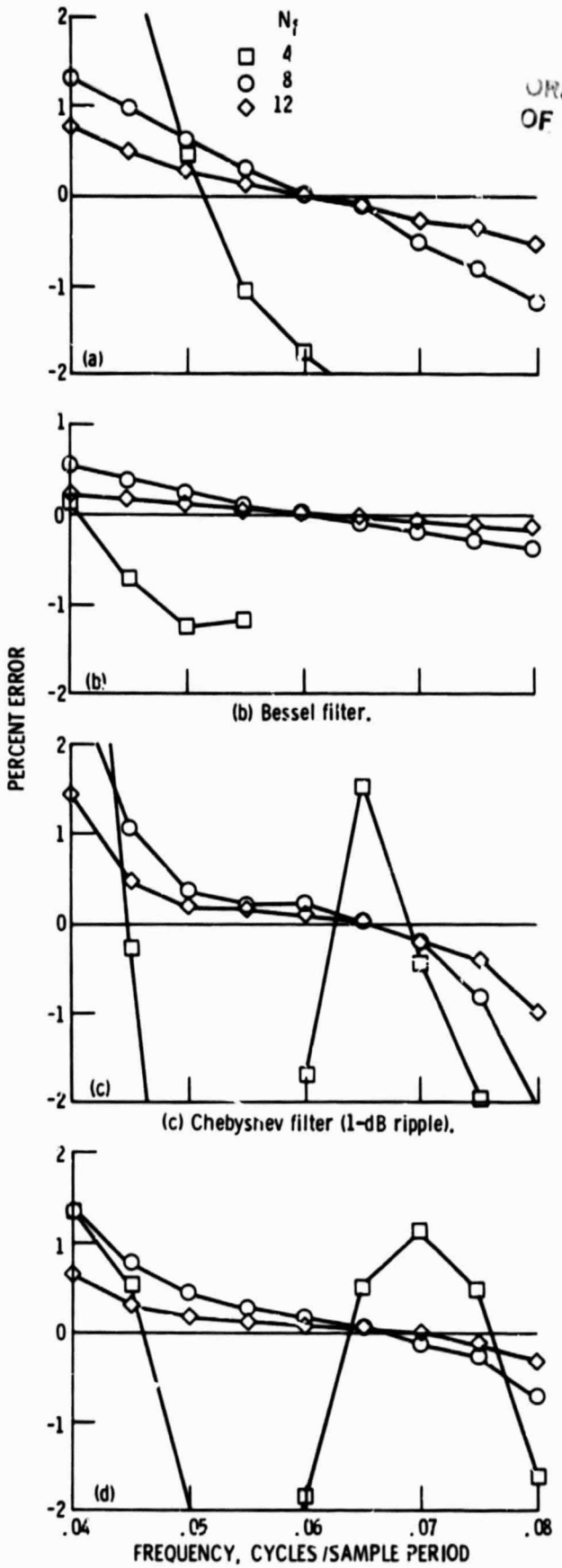

Fig. 5 Percent error as function of frequency of the averages of four fringes (N_c = 4)

(a) Butterworth filter
(b) Bessel filter
(c) Chebyshev filter (1-dB ripple)
(d) Chebyshev filter (0.1-dB ripple)

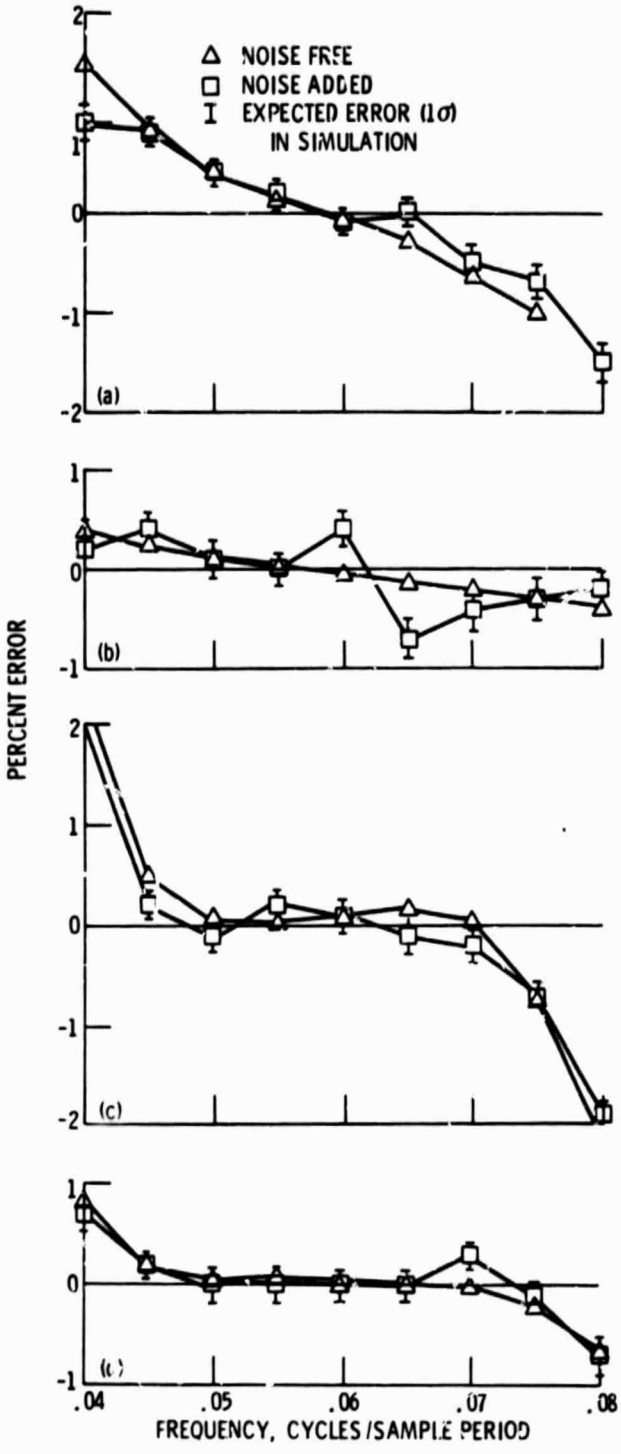

Fig. 6 Percent error as function of frequency of the averages of four fringes (N_f = 8, N_c = 4) for normally distributed random amplitude signals

(a) Butterworth filter
(b) Bessel filter
(c) Chebyshev filter (1-dB ripple
(d) Chebyshev filter (0.1-dB ripple)

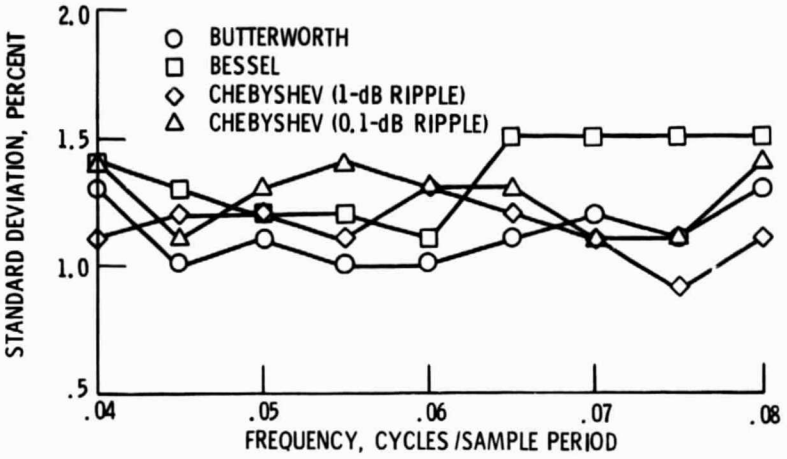

Fig. 7 Standard deviation of the measurement of frequency as function of frequency of the average of four fringes (N_f = 8, N_c = 4) for normally distributed random amplitude signals with noise added

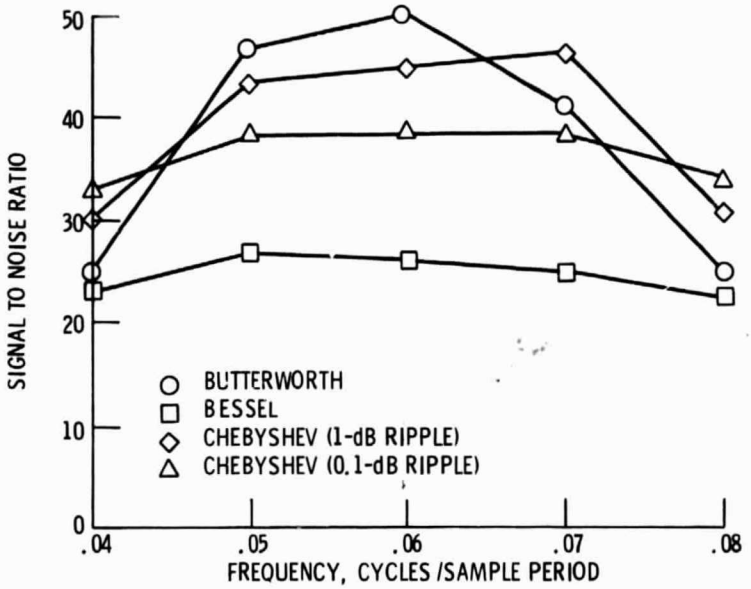

Fig. 8 Signal to noise ratio as function of frequency for A_s = 15 counts/sample period, A_{dc} = 10 counts/sample period, noise-added signals

1. Report No.	2. Government Accession No.	3. Recipient's Catalog No.
NASA TM-87047		

4. Title and Subtitle	5. Report Date
Filter Induced Errors in Laser Anemometer Measurements Using Counter Processors	6. Performing Organization Code: 533-04-1A

7. Author(s)	8. Performing Organization Report No.
Lawrence G. Oberle and Richard G. Seasholtz	E-2609
	10. Work Unit No.

9. Performing Organization Name and Address	11. Contract or Grant No.
National Aeronautics and Space Administration Lewis Research Center Cleveland, Ohio 44135	13. Type of Report and Period Covered: Technical Memorandum

12. Sponsoring Agency Name and Address	14. Sponsoring Agency Code
National Aeronautics and Space Administration Washington, D.C. 20546	

15. Supplementary Notes

Prepared for the International Laser Anemometry Symposium, ASME Winter Annual Meeting, Miami, Florida, November 17-21, 1985.

16. Abstract

Previous simulations of laser Doppler anemometer (LDA) systems have focused primarily on noise studies or biasing errors. Another possible source of error is due to the choice of filter types and filter cutoff frequencies. In general, before it is applied to the counter portion of the signal processor, a Doppler burst is filtered to remove the pedestal and to reduce noise in the frequency bands outside the region in which the signal occurs. Filtering, however, can introduce errors into the measurement of the frequency of the input signal which leads to inaccurate results. With the results of this paper it is possible to evaluate errors caused by signal filtering in an LDA counter-processor data acquisition system and to choose filters for a specific application which will reduce these errors.

17. Key Words (Suggested by Author(s))	18. Distribution Statement
Laser anemometry	Unclassified - unlimited STAR Category 35

19. Security Classif. (of this report)	20. Security Classif. (of this page)	21. No. of pages	22. Price*
Unclassified	Unclassified		

*For sale by the National Technical Information Service, Springfield, Virginia 22161